文章编号：1001-9014(2021)05-0589-06　　DOI：10. 11972/j. issn. 1001-9014. 2021. 05. 004

一维光子准晶平V透镜

郭嘉威，谭　威，谢建斓，刘建军*

（湖南大学 物理与微电子科学学院，微纳光电器件及应用教育部重点实验室，低维结构物理与器件湖南省重点实验室，湖南 长沙 410082）

摘要：一维光子准晶已在亚波长、亚衍射聚焦及超分辨成像领域不断展现优越性。为丰富及拓展其聚焦特性的应用，本文提出了一种一维光子准晶平V透镜，并研究了材料厚度对其聚焦特性的影响。研究结果表明，该透镜可在第二能带较宽的波长范围内实现亚波长及亚衍射聚焦。本文研究结果将为一维光子准晶平V透镜的设计及应用提供参考。

关　键　词：光子准晶；透镜；亚波长聚焦；亚衍射聚焦

中图分类号：O734　　**文献标识码**：A

One-dimensional photonic quasi-crystal plano-V lens

GUO Jia-wei，　TAN Wei，　XIE Jian-lan，　LIU Jian-jun*

（Key Laboratory for Micro/Nano Optoelectronic Devices of Ministry of Education & Hunan Provincial Key Laboratory of Low-Dimensional Structural Physics and Devices，School of Physics and Electronics，Hunan University，Changsha 410082，China）

Abstract：One-dimensional photonic quasi-crystal（1D PQC）has continuously shown their superiority in the fields of sub-wavelength focusing，sub-diffraction focusing and super-resolution imaging. In order to enrich and expand the application of its focusing characteristics，a 1D PQC plano-V lens is proposed and the effect of material thickness on its focusing characteristics is studied in this paper. The results show that the lens can achieve sub-wavelength focusing and sub-diffraction focusing in a wide wavelength range of the second band. The results in this paper will provide reference for the design and application of 1D PQC plano-V lens.

Key words：photonic quasi-crystal，lens，sub-wavelength focusing，sub-diffraction focusing

引言

随着集成光学及微纳光子学的不断发展[1-11]，微透镜与微透镜阵列[12-15]因其体积小、重量轻、便于集成化及阵列化等优点而成为研究热点。光子晶体透镜作为微透镜的杰出代表之一，在亚波长、亚衍射聚焦及超分辨率成像方面具有良好的性能[16-20]，且准周期光子晶体（又称为光子准晶）透镜的聚焦及成像特性[21-27]优于周期光子晶体透镜。

光子准晶因具有特殊的结构特征（如：二维光子准晶具有长程有序性、旋转对称性、自相似性[28-30]；一维光子准晶具有 Fibonacci 序列[31-33]、Thue-Morse序列结构[34-36]）而使其散射子具有多种位置特征。因此，与周期光子晶体[37-38]相比，光子准晶在设计过程中可调节的参数更多，且可实现广泛应用，如：透镜[21-27]、光纤[39-47]、棱镜[48]、滤波器[39,49-50]、传感器[43,46,51-52]、空芯光束的产生[53]及拓扑光子器件[54]等。目前，光子准晶透镜亚波长、亚衍射聚焦及超分辨成像的研究主要集中于二维光子准晶[21-24,27]，而一维光子准晶透镜的研究则相对薄弱。相对于二维光子准晶结构，一维光子准晶结构更简单，在制作上也相对容易，便于推广应用。另外，与当前研究较多的超表面平面透镜[55-56]相比，一维光子准晶透镜也具有一定优势。超表面平面透镜一般是二维结构，制备较复杂，且其周期结构使得制备误差对光学性能影响较大，而一维光子准晶

收稿日期：2020-12-10，**修回日期**：2021-07-14　　**Received date**：2020-12-10，**Revised date**：2021-07-14

基金项目：国家自然科学基金青年科学基金项目（61405058）及面上项目（62075059），湖南省自然科学基金面上项目（2017JJ2048，2020JJ4161）.

作者简介（Biography）：郭嘉威，男，湖南益阳人，本科生，主要研究领域为光子准晶器件，Email：jiawei_guo_hnu@163. com.

*通讯作者（Corresponding author）：Email：jianjun. liu@hnu. edu. cn.

透镜则可避免这些问题。虽我们已开展了一维光子准晶的聚焦特性研究，但仅限于平凹透镜[25-26]及圆形光栅[57]。为丰富及拓展一维光子准晶聚焦特性的应用，其它结构的一维光子准晶透镜尚待研究。

本文提出了一种V形Fibonacci光子准晶透镜，分析了聚焦特性随电介质厚度变化的规律。

1 模型与算法

传统光学透镜的分辨率受Rayleigh衍射极限的限制。倏逝波在穿过传统光学透镜后呈指数衰减而不能到达成像面参与成像，其携带的物方信息被丢失。光子晶体作为一种人工微结构材料，其在第二通带可实现负折射，从而增强倏逝波的振幅，修复倏逝波的相位，提高透镜的分辨率[16-20]，从而实现亚波长聚焦。类比周期光子晶体，光子准晶在第二通带也会发生负折射[25-26]。这种具有传播和增强倏逝波性能的透镜可提高成像分辨率及聚焦效果。

在数学上，Fibonacci序列是指：1、1、2、3、5、8、13、21、34、……。在形式上，Fibonacci序列可用递推的形式定义：F(0)=0，F(1)=1，F(2)=1，F(m)=F(m−1)+F(m−2)(m≥2，m∈N)[58]。若把两种不同介质材料（设为A、B）按Fibonacci序列排布即可构成Fibonacci光子准晶。如图**1**(**a**)，若m取不同的数值，则可得到不同的Fibonacci光子准晶。设F(0)=B，F(1)=A，则F(2)= F(1)+ F(0)=AB，F(3)= F(2)+ F(1)=ABA，F(4)= F(3)+ F(2)=ABAAB……。根据现实功能需要，取不同材料、厚度、层数及外形结构与尺寸，可设计不同的Fibonacci光子准晶器件（如本文设计的一维光子准晶平V透镜，如图**1**(**b**)）。

如图**1**(**a**)，设电介质材料A、B分别为SiO_2、Ge，其折射率分别为n_A=1.56，n_B=4.00，其厚度分别为d_A、d_B。透镜的横截面，如图**1**(**b**)所示，其宽度、高度、V形平台宽度及底座高度分别设为L、h、L_1、h_1。V形坡面采用光栅结构。平面光波从透镜底部入射，并汇聚于透镜上方。设焦点半宽度（full width at half maximum）FWHM=$\eta\lambda$，系数η值越小，其焦点质量越好。

为了研究透镜的聚焦特性，首先需分析透镜的光子能带结构，以得到可在透镜中传输的波长范围。因光子准晶不具有周期结构（平移对称性），故其能带结构不可用色散关系表征，本文采用透射谱表征其能带结构。通过传输矩阵法，首先计算光子准晶的透射系数[59]。对于TE模式，由于介质A的厚

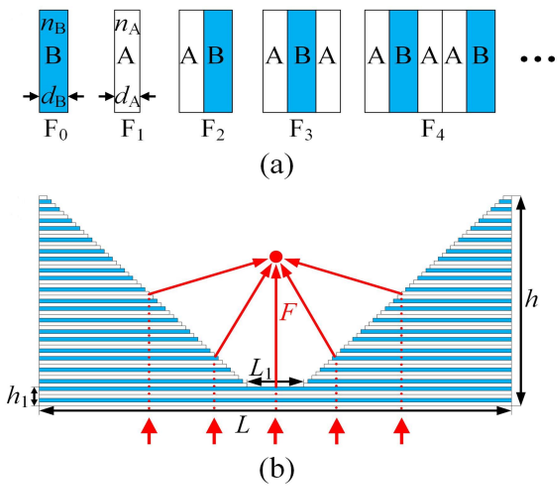

图1 （a）具有Fibonacci序列的结构示意图（b）Fibonacci光子准晶平V透镜的二维模型，红色箭头表示平面波的入射方向及穿过透镜后汇聚到焦点的过程，F为透镜的焦距

Fig. 1 （a）Structure diagram with the Fibonacci sequence（b）2D model of the Fibonacci photonic quasi-crystals（PQC）plano-V lens. The red arrows indicate the incident direction of the plane wave and the process of converging to the focal point after passing through the lens. F is the focal distance of the lens

度为d_A=100nm不变，其传输矩阵M_A可由下式表示：

$$M_A=\begin{bmatrix}\cos\delta_A & \frac{i}{\eta_A}\sin\delta_A\\ i\eta_A\sin\delta_A & \cos\delta_A\end{bmatrix}. \tag{1}$$

介质B的厚度在d_B∈[10nm，300nm]范围内变化，所以其传输矩阵M_{Bj}(j∈[10，300]，步长Δj=5，不同的j值对应不同厚度下的介质B)可由下式表示：

$$M_{Bj}=\begin{bmatrix}\cos\delta_{Bj} & \frac{i}{\eta_{Bj}}\sin\delta_{Bj}\\ i\eta_{Bj}\sin\delta_{Bj} & \cos\delta_{Bj}\end{bmatrix}, \tag{2}$$

其中

$$\delta_k=\frac{-2\pi}{\lambda}n_k d_k\cos\theta_t(k=A,Bj), \tag{3}$$

$$\eta_k=\sqrt{\frac{\varepsilon_0}{\mu_0}}n_k\cos\theta_t(k=A,Bj), \tag{4}$$

其中δ_k、η_k、d_k、λ、n_k、ε_0和μ_0分别是相位差、有效光导纳、电介质厚度、真空波长、电介质折射率、真空介电常数和磁导率。

当入射平面波穿过N层介质后，透射系数可表示为：

$$t=\frac{2\eta_0}{A\eta_0+B\eta_0\eta_N+1+C+D\eta_N+1}, \tag{5}$$

透射率可表示为:

$$T = t^2 . \tag{6}$$

对于TM模式,表达式(5)和(6)同样适用,表达式(4)需要改为:

$$\eta_k = \sqrt{\frac{\varepsilon_0}{\mu_0}} n_k \Big/ \cos\theta_t \ (k = A, Bj) . \tag{7}$$

由于本文中入射平面波均为垂直入射,折射角θ_t均为0,即TE模式下和TM模式下的透射率T相等,即本文提出的一维光子准晶平V透镜,入射平面光波的偏振方向并不影响透镜的聚焦效果。通过上述方法,可计算得到透镜(d_A=d_B=100nm)的透射谱,如图2所示。

由图2可知,Fibonacci序列的光子准晶可产生

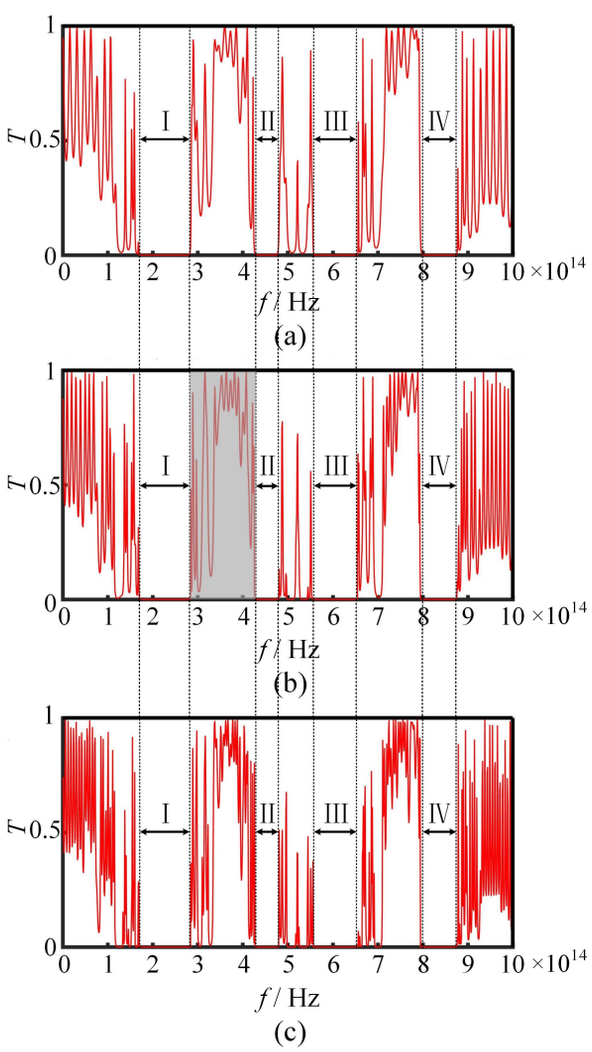

图2　具有不同Fibonacci序列的光子准晶的透射谱:(a) F(8) (b) F(9) (c) F(10)

Fig. 2　Transmission spectrum of a PQC with different Fibonacci sequences: (a) F(8) (b) F(9) (c) F(10)

四大带隙(见区域:Ⅰ、Ⅱ、Ⅲ、Ⅳ),其所在的频率范围分别为$f_{Ⅰ}$∈[1.717×10^{14}Hz, 2.832×10^{14} Hz],$f_{Ⅱ}$∈[4.293×10^{14}Hz, 4.786×10^{14} Hz], $f_{Ⅲ}$ ∈[5.578×10^{14}Hz, 6.542×10^{14} Hz],$f_{Ⅳ}$∈[7.961×10^{14}Hz, 8.753×10^{14} Hz]。F(8)中各带隙边缘存在些许弯曲,即带隙尚未完全成形。F(9)中各带隙边缘无弯曲,即带隙已完全成形。随着光子准晶层数的进一步增加,F(10)中各带隙边缘无弯曲,虽带隙保持稳定,但相对于F(9),其层数增加接近1倍,导致制备成本及难度大幅度增加。因此,选用F(9)作为透镜的序列数,既能达到较好的聚焦效果,又能节省材料且方便制备。

本文采用有限元法计算分析Fibonacci光子准晶平V透镜的聚焦特性。

2　结果与讨论

进一步仿真计算发现,在F(9)序列光子准晶的第二通带频段(见图2(**b**)灰色区域,f_{focus}∈[2.832×10^{14} Hz, 4.293×10^{14}Hz](此时d_B=100 nm))可发生聚焦。不过,实际制备误差将导致聚焦频率发生偏离。为此,改变d_B∈[50 nm, 200 nm],可计算得到透镜对入射平面波的公共聚焦波段范围。以d_B=50nm、100nm、200nm为例,透射光谱如图3所示。

当d_B取不同值时,透镜对入射平面波的聚焦频率范围如下:当d_B=50 nm时,f∈[3.139×10^{14} Hz, 4.858×10^{14}Hz];当d_B=100 nm时,f∈[2.832×10^{14} Hz, 4.293×10^{14}Hz];当d_B=200 nm时,f∈[2.742×10^{14} Hz, 4.135×10^{14}Hz]。因此,公共聚焦频率范围为f_{cfocus}∈[3.139×10^{14} Hz, 4.135×10^{14}Hz](见图3灰色区域)。从该频段中取平面波f=3.989×10^{14} Hz(对应波长λ=752 nm),研究材料厚度变化对透镜聚焦特性的影响。固定材料SiO_2的厚度d_A=100 nm,且以Δd_B=5 nm为间隔改变材料Ge的厚度d_B∈[10 nm, 300nm],焦点的归一化焦点强度、FWHM系数η及焦距随d_B变化的规律,如图4所示。

由图4可知,随着d_B的增加,焦点的归一化焦点强度、FWHM系数η及焦距均呈振荡趋势。由图(**a**)可知,在d_B=10 nm、100 nm、185 nm、265 nm、275 nm时,焦点强度取得局部最大值。由图(**b**)可知,当d_B∈[20 nm, 65 nm]时,0.5λ<FWHM<λ,透镜实现了亚波长聚焦,而其它情况下,FWHM<0.5λ,突破了衍射极限,也即透镜实现了亚衍射聚焦。由图(**c**)可知,当d_B=80nm、185nm时,焦距取得局部最大值。综合图4可知,当d_A=d_B=100nm时,焦点强度最

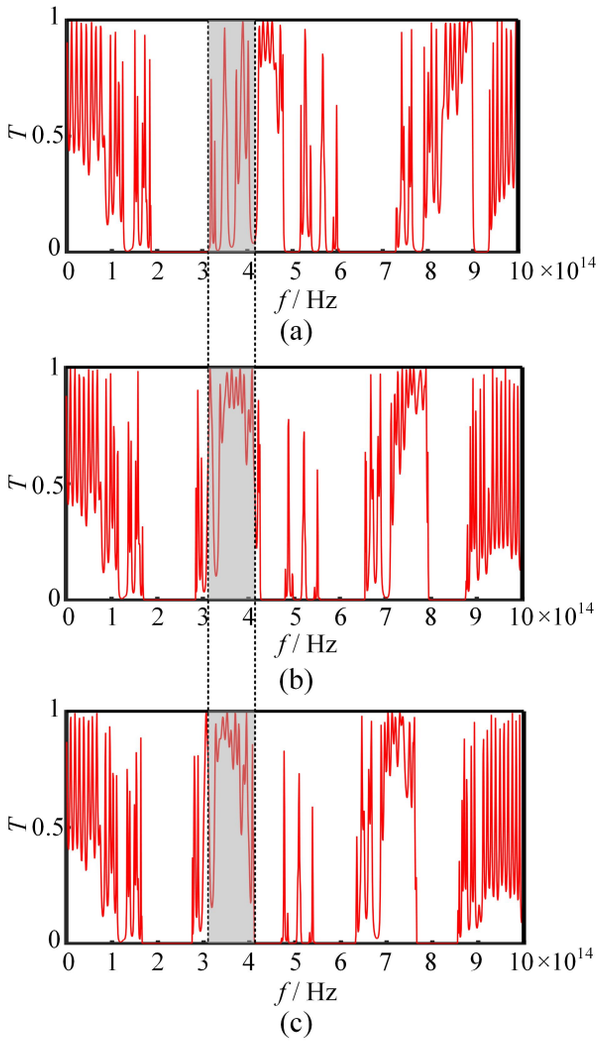

图3 d_A=100nm，d_B变化时Fibonacci光子准晶的透射谱：(a) d_B=50nm (b) d_B=100 nm (c) d_B=200 nm

Fig. 3 Transmission spectrum of a PQC when d_A=100 nm and d_B changes: (a) d_B=50 nm (b) d_B=100nm (c) d_B=200 nm

大，且FWHM=0.367λ趋于最小，实现了最佳的亚衍射聚焦特性，如图5所示。

由图5可知，一维光子准晶平V透镜的聚焦点低于V形高度，使该透镜在超导纳米线单光子探测领域具有重要的潜在应用。超导纳米线单光子探测器的探测效率与纳米线对光子的吸收率密切相关，提高纳米线对光子的吸收率即可提高探测器的探测效率[60]。若将超导纳米线单光子探测器的纳米线直接制作在透镜的V形凹槽内部，使纳米线置于透镜焦点处，则大部分的光子汇集于纳米线上，从而可大幅提升探测器的探测效率。另外，相较于一维光子准晶平凹透镜[25-26]，本文提出的一维光子准晶平V透镜最佳焦点的半高宽FWHM更小，焦点

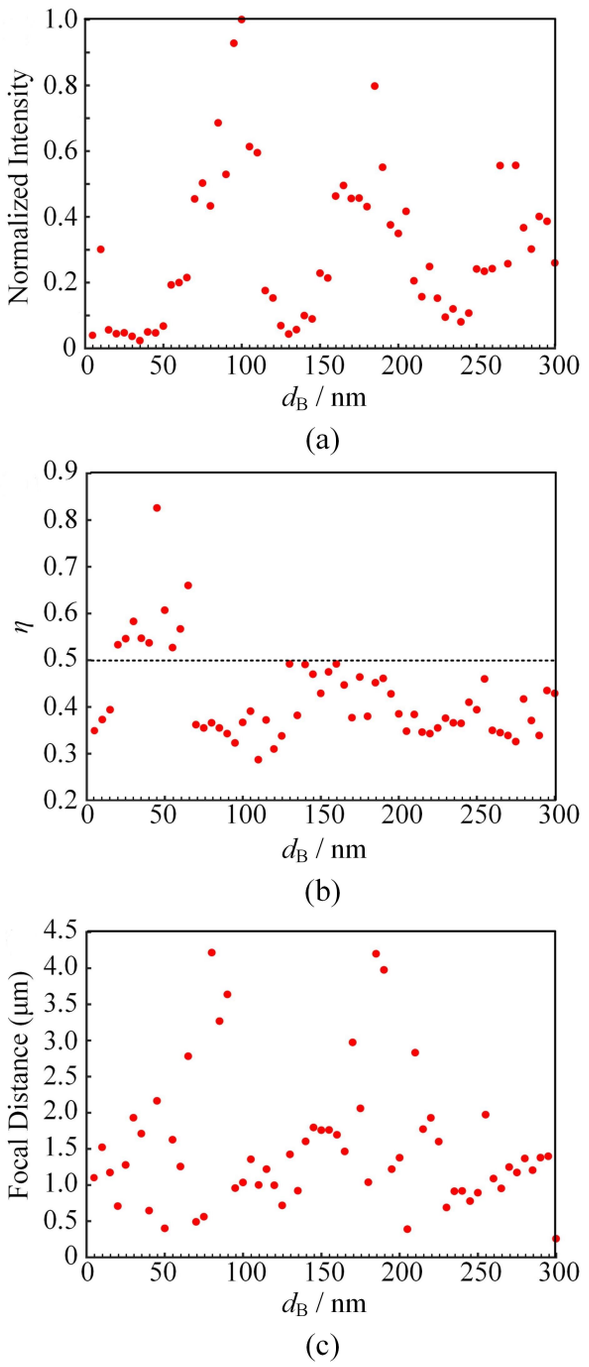

图4 Fibonacci光子准晶平V透镜在λ=752nm且d_B变化时的聚焦特性：(a)归一化焦点强度 (b)FWHM 系数 η；(c)焦距

Fig. 4 The focusing characteristics of Fibonacci PQC plano-V lens when λ=752nm and d_B varies: (a) normalized intensity of focus, (b) FWHM coefficient η, and (c) focal distance

旁瓣更小，且该透镜可调参数更多，这意味着可以更加细微地去调节透镜结构，从而实现更好的亚波长、亚衍射聚焦效果。

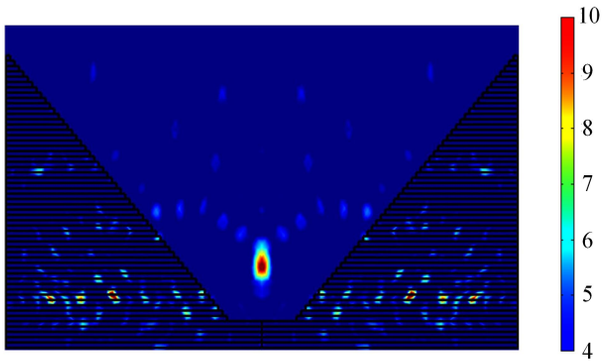

图5　d_A=d_B=100 nm的Fibonacci光子准晶平V透镜对平面波λ=752nm的聚焦场

Fig. 5　Focusing field of the Fibonacci PQC plano-V lens with d_A=d_B=100 nm for a plane wave λ =752nm

3　结论

提出了一种Fibonacci序列光子准晶平V透镜，并分析了透镜随电介质材料厚度变化的亚波长、亚衍射聚焦特性。该透镜可以在一个较宽波长范围内实现亚波长、亚衍射聚焦。研究结果可为一维光子准晶平V透镜的材料选择、结构设计及应用提供参考。

References

[1] Wang Z, Su K, Feng B, *et al*. Coupling length variation and multi-wavelength demultiplexing in photonic crystal waveguides[J]. *Chin. Opt. Lett.*, 2018, **16**(1): 48-52.

[2] Pang Z, Tong H, Wu X, *et al*. Theoretical study of multiexposure zeroth-order waveguide mode interference lithography[J]. *Opt. Quant. Electron.*, 2018, **50**(9): 335.

[3] Tong H, Xu Y, Su Y, *et al*. Theoretical study for fabricating elliptical subwavelength nanohole arrays by higher-order waveguide-mode interference[J]. *Results Phys.*, 2019, **14**: 102460.

[4] Wang X, Zhu J, Wen X, *et al*. Wide range refractive index sensor based on a coupled structure of Au nanocubes and Au film[J]. *Opt. Mater. Express*, 2019, **9**(7): 3079-3088.

[5] Wang X, Pang Z, Yang H, *et al*. Theoretical study of subwavelength circular grating fabrication based on continuously exposed surface plasmon interference lithography[J]. *Results Phys.*, 2019, **14**: 102446.

[6] Chen J, Wang X, Tang F, *et al*. Substrates for surface-enhanced Raman spectroscopy based on TiN plasmonic antennas and waveguide platforms[J]. *Results Phys.*, 2020, **16**: 102867.

[7] Li J, Chen X, Yi Z, *et al*. Broadband solar energy absorber based on monolayer molybdenum disulfide using tungsten elliptical arrays [J]. *Mater. Today Energy*, 2020, **16**: 100390.

[8] Wu H, Jile H, Chen Z, *et al*. Fabrication of ZnO@ MoS_2 Nanocomposite heterojunction arrays and their photoelectric properties[J]. *Micromachines*, 2020, **11**(2): 189.

[9] Li J, Chen Z, Yang H, *et al*. Tunable broadband solar energy absorber based on monolayer transition metal dichalcogenides materials using Au nanocubes[J]. *Nanomaterials*, 2020, **10**(2): 257.

[10] Wang Y, Chen Z, Xu D, *et al*. Triple-band perfect metamaterial absorber with good operating angle polarization tolerance based on split ring arrays [J]. *Results Phys.*, 2020, **16**: 102951.

[11] Qin F, Chen Z, Chen X, *et al*. A tunable triple-band near-infrared metamaterial absorber based on Au nanocuboids array[J]. *Nanomaterials*, 2020, **10**(2): 207.

[12] Kamali S M, Arbabi E, Arbabi A, *et al*. A review of dielectric optical metasurfaces for wavefront control [J]. *Nanophotonics*, 2018, **7**(6): 1041-1068.

[13] Qiao P, Yang W, Chang-Hasnain C J. Recent advances in high-contrast metastructures, metasurfaces, and photonic crystals [J]. *Adv. Opt. Photonics.*, 2018, **10**(1): 180-245.

[14] Zuo H, Yang W, Zhang J, *et al*. Focal shift of silicon microlens array in mid-infrared regime[J]. J. *Infrared Millim. Waves*, 2017, **36**(2): 149-153.

[15] Tian Y, Tan Z, Han X, *et al*. Phononic crystal lens with an asymmetric scatterer [J]. *J. Phys. D: Appl. Phys.*, 2018, **52**(2): 025102.

[16] Xie J, Wang J, Ge R, *et al*. Multiband super-resolution imaging of graded-index photonic crystal flat lens [J]. *J. Phys. D: Appl. Phys.*, 2018, **51**(20): 205103.

[17] Zhou T, Tan W, Yan B, *et al*. Sub-wavelength focusing in the visible wavelength range realized by a one-dimensional ternary photonic crystal plano-concave lens[J]. *Superlattice. Microst.*, 2018, **124**: 176-184.

[18] Liang S, Xie J, Tang P, *et al*. Large object distance and super-resolution graded-index photonic crystal flat lens [J]. *Opt. Express*, 2019, **27**(7): 9601-9609.

[19] Cen Y, Xie J, Liu J. Multi-band imaging and focusing of photonic crystal flat lens with scatterer-size gradient [J]. *Chin. Opt. Lett.*, 2019, **17**(8): 080501.

[20] Sheng J, Xie J, Liu J. Multiple super-resolution imaging in the second band of gradient lattice spacing photonic crystal flat lens [J]. *Chin. Opt. Lett.*, 2020, **18**(12): 120501.

[21] Feng Z, Zhang X, Wang Y, *et al*. Negative refraction and imaging using 12-fold-symmetry quasicrystals [J]. *Phys. Rev. Lett.*, 2005, **94**(24): 247402.

[22] Zhang X, Li Z, Cheng B, *et al*. Non-near-field focus and imaging of an unpolarized electromagnetic wave through high-symmetry quasicrystals [J]. *Opt. Express*, 2007, **15**(3): 1292-1300.

[23] Liu J, Liu E, Fan Z. Width dependence of two-dimensional photonic quasicrystal flat lens imaging characteristics[J]. *J. Mod. Optic.*, 2016, **63**(7): 692-696.

[24] Liu J, Fan Z. Size limits for focusing of two-dimensional photonic quasicrystal lenses[J]. *IEEE Photonic. Tech. L.*, 2018, **30**(11): 1001-1004.

[25] Tan W, Liu E, Yan B, *et al*. Subwavelength focusing of a cylindrically symmetric plano-concave lens based on a one-dimensional Thue-Morse photonic quasicrystal [J]. *Appl. Phys. Express*, 2018, **11**(9): 092002.

[26] Zhang W, Tan W, Yang Q, *et al*. Subwavelength focusing in visible light band by a Fibonacci photonic quasi-crystal plano-concave lens [J]. *J. Opt. Soc. Am. B*, 2018, **35**(10): 2364-2367.
[27] Zhao H, Xie J, Liu J. An approximate theoretical explanation for super-resolution imaging of two-dimensional photonic quasi-crystal flat lens [J]. *Appl. Phys. Express*, 2020, **13**(2): 022007.
[28] Chan Y, Chan C, Liu Z. Photonic band gaps in two dimensional photonic quasicrystals [J]. *Phys. Rev. Lett.*, 1998, **80**(5): 956-959.
[29] Shechtman D G, Blech I A, Gratias D, *et al*. Metallic phase with long-range orientational order and no translational symmetry [J]. *Phys. Rev. Lett.*, 1984, **53**(20): 1951-1953.
[30] Xi X Y, Sun X H. Photonic bandgap properties of two dimensional photonic quasicrystals with multiple complex structures [J]. *Superlattice. Microst.*, 2019, **129**: 247-251.
[31] Capaz R B, Koiller B, de Queiroz S L A. Gap states and localization properties of one-dimensional Fibonacci quasicrystals[J]. *Phys. Rev. B*, 1990, **42**(10): 6402-6407.
[32] Gellermann W, Kohmoto M, Sutherland B, *et al*. Localization of light waves in Fibonacci dielectric multilayers [J]. *Phys. Rev. Lett.*, 1994, **72**(5): 633-636.
[33] Bian L, Liu P, Li G. Design of tunable devices using one-dimensional Fibonacci photonic crystals incorporating graphene at terahertz frequencies [J]. *Superlattice. Microst.*, 2016, **98**: 522-534.
[34] Jiang X, Zhang Y, Feng S, *et al*. Photonic band gaps and localization in the Thue - Morse structures[J]. *Appl. Phys. Lett.*, 2005, **86**(20): 201110.
[35] Liu N. Propagation of light waves in Thue-Morse dielectric multilayers [J]. *Phys. Rev. B*, 1997, **55**(6): 3543-3547.
[36] Dal Negro L, Stolfi M, Yi Y, *et al*. Photon band gap properties and omnidirectional reflectance in Si/ SiO_2 Thue - Morse quasicrystals[J]. *Appl. Phys. Lett.*, 2004, **84**(25): 5186-5188.
[37] Fang Y. Imaging by photonic crystal without negative refraction[J]. *Laser Phys. Lett.*, 2005, **2**(10): 502-505.
[38] Fang Y, Ouyang Z. Realization of absolute negative refraction index by a photonic crystal using anisotropic dielectric material[J]. *Chin. Opt. Lett.*, 2008, **6**(1): 57-60.
[39] Yan B, Wang A, Liu E, *et al*. Polarization filtering in the visible wavelength range using surface plasmon resonance and a sunflower-type photonic quasi-crystal fiber [J]. *J. Phys. D: Appl. Phys.*, 2018, **51**(15): 155105.
[40] Liu E, Yan B, Tan W, *et al*. Guiding characteristics of sunflower-type fiber [J]. *Superlattice. Microst.*, 2018, **115**: 123-129.
[41] Liu E, Tan W, Yan B, *et al*. Broadband ultra-flattened dispersion, ultra-low confinement loss and large effective mode area in an octagonal photonic quasi-crystal fiber[J]. *J. Opt. Soc. Am. A*, 2018, **35**(3): 431-436.
[42] Han J, Liu E, Liu J. Circular gradient-diameter photonic crystal fiber with large mode area and low bending loss[J]. *J. Opt. Soc. Am. A*, 2019, **36**(4): 533-539.
[43] Liu Q, Yan B, Liu J. U-shaped photonic quasi-crystal fiber sensor with high sensitivity based on surface plasmon resonance[J]. *Appl. Phys. Express*, 2019, **12**(5): 052014.
[44] Liu E, Liang S, Liu J. Double-cladding structure dependence of guiding characteristics in six-fold symmetric photonic quasi-crystal fiber[J]. *Superlattice. Microst.*, 2019, **130**: 61-67.
[45] Liu E, Tan W, Yan B, *et al*. Robust transmission of orbital angular momentum mode based on a dual-cladding photonic quasi-crystal fiber [J]. J. *Phys. D Appl. Phys.*, 2019, **52**(32): 325110.
[46] Li C, Yan B, Liu J. Refractive index sensing characteristics in a D-shaped photonic quasi-crystal fiber sensor based on surface plasmon resonance[J]. *J. Opt. Soc. Am. A*, 2019, **36**(10): 1663-1668.
[47] Huo Z, Liu E, Liu J. Hollow-core photonic quasicrystal fiber with high birefringence and ultra-low nonlinearity [J]. *Chin. Opt. Lett.*, 2020, **18**(3): 030603.
[48] Liu J, Tan W, Liu E, *et al*. Planar scanning method for detecting refraction characteristics of two-dimensional photonic quasi-crystal wedge-shaped prisms[J]. *J. Opt. Soc. Am. A*, 2016, **33**(5): 978-983.
[49] Zhao Y, Wang Z, Jiang Z, *et al*. Add-drop filter with compound structures of photonic crystal and photonic quasicrystal [J]. J. *Infrared Millim. Waves*, 2017, **36**(3): 342-348.
[50] Ren J, Sun X H, Wang S. A narrowband filter based on 2D 8-fold photonic quasicrystal[J]. *Superlattice. Microst.*, 2018, **116**: 221-226.
[51] Ge R, Xie J, Yan B, *et al*. Refractive index sensor with high sensitivity based on circular photonic crystal [J]. *J. Opt. Soc. Am. A*, 2018, **35**(6): 992-997.
[52] Shi A, Ge R, Liu J. Refractive index sensor based on photonic quasi-crystal with concentric ring microcavity [J]. *Superlattice. Microst.*, 2019, **133**: 106198.
[53] Feng B, Liu E, Wang Z, *et al*. Generation of terahertz hollow beams by a photonic quasi-crystal flat lens [J]. *Appl. Phys. Express*, 2016, **9**(6): 062003.
[54] Yan B, Xie J, Liu E, *et al*. Topological edge state in the two-dimensional Stampfli-triangle photonic crystals [J]. *Phys. Rev. Applied*, 2019, **12**(4): 44004.
[55] Arbabi E, Arbabi A, Kamali S M, *et al*. MEMS-tunable dielectric metasurface lens [J]. *Nat. Commun.*, 2018, **9**(1): 1-9
[56] Xie J, Liang S, Liu J, *et al*. Near-zero-sidelobe optical subwavelength asymmetric focusing lens with dual-layer metasurfaces[J]. *Ann. Phys.*, 2020, **532**(7): 2000035.
[57] Zhang C, Jiang Z, Tan W, *et al*. Non-near-field sub-diffraction focusing in the visible wavelength range by a Fibonacci subwavelength circular grating[J]. *J. Opt. Soc. Am. A*, 2018, **35**(10): 1701-1704.
[58] Horadam A F. A generalized Fibonacci sequence[J]. *Amer. Math. Monthly*, 1961, **68**(5): 455-459.
[59] Yue C, Tan W, Liu J. Photonic band gap properties of one-dimensional Thue-Morse all-dielectric photonic quasicrystal[J]. *Superlattice. Microst.*, 2018, **117**: 252-259.
[60] Yamashita T, Miki S, Terai H, *et al*. Low-filling-factor superconducting single photon detector with high system detection efficiency [J]. *Opt. Express*, 2013, **21**(22): 27177-27184.